

LETTER TO THE EDITOR

Refinement of the convex shape model and tumbling spin state of (99942) Apophis using the 2020-2021 apparition data

H.-J. Lee¹, M.-J. Kim¹, A. Marciniak², D.-H. Kim^{1,3}, H.-K. Moon¹, Y.-J. Choi^{1,4}, S. Zoła⁵, J. Chatelain⁷, T. A. Lister⁷, E. Gomez⁸, S. Greenstreet^{9,10}, A. Pál¹¹, R. Szakáts¹¹, N. Erasmus¹², R. Lees¹³, P. Janse van Rensburg^{12,13}, W. Ogłóża⁶, M. Drózd⁶, M. Żejmo¹⁴, K. Kamiński², M. K. Kamińska², R. Duffard¹⁵, D.-G. Roh¹, H.-S. Yim¹, T. Kim¹⁶, S. Mottola¹⁷, F. Yoshida^{18,19}, D. E. Reichart²⁰, E. Sonbas²¹, D. B. Caton²², M. Kaplan²³, O. Erece^{23,24}, and H. Yang¹

(Affiliations can be found after the references)

Received ; accepted

ABSTRACT

Context. The close approach of the near-Earth asteroid (99942) Apophis to Earth in 2029 will provide a unique opportunity to examine how the physical properties of the asteroid could be changed due to the Earth's gravitational perturbation. As a result, the Republic of Korea is planning a rendezvous mission to Apophis.

Aims. Our aim was to use photometric data from the apparitions in 2020-2021 to refine the shape model and spin state of Apophis.

Methods. Using thirty-six 1 to 2-m class ground-based telescopes and the Transiting Exoplanet Survey Satellite, we performed a photometric observation campaign throughout the 2020-2021 apparition. The convex shape model and spin state were refined using the light-curve inversion method.

Results. According to our best-fit model, Apophis is rotating in a short axis mode with rotation and precession periods of 264.178 hours and 27.38547 hours, respectively. The angular momentum vector orientation of Apophis was found as $(275^\circ, -85^\circ)$ in the ecliptic coordinate system. The ratio of the dynamic moments of inertia of this asteroid was fitted to $I_a : I_b : I_c = 0.64 : 0.97 : 1$, which corresponds to an elongated prolate ellipsoid. These findings regarding the spin state and shape model could be used to not only design the space mission scenario but also investigate the impact of the Earth's tidal force during close encounters.

Key words. Minor planets, asteroids: individual: (99942) Apophis – Techniques: photometric

1. Introduction

The Aten-type near-Earth asteroid (99942) Apophis (2004 MN₄) (hereafter Apophis) is an Sq-type asteroid with an estimated size of 340 m (Binzel et al. 2009; Brozović et al. 2018; Reddy et al. 2018). This asteroid was discovered on June 19, 2004, by R.A. Tucker, D.J. Tholen, and F. Bernardi at Kitt Peak, Arizona. From early prediction, it was estimated that this asteroid could impact Earth with a maximum probability of 2.7% (JPL Sentry on December 27, 2004; Chesley 2006). As the accuracy of the orbital prediction improved in follow-up observations, the impact probability of Apophis was reduced. In particular, the prediction derived from high-precision radar observations at the Arecibo Observatory in 2005 and 2006 indicated that this asteroid will pass by Earth at a geocentric distance of 38,326 km (approximately 6 Earth radii), which is within the geosynchronous orbit in April 2029 (Giorgini et al. 2008). Recently, the radar observations at the Goldstone Solar System Radar (GSSR) and Green Bank Telescope (GBT) in March 2021 have precisely estimated Apophis' orbit around the Sun, ruling out any Earth impact threat for the next hundred years or more (Greicius 2021).

Although Apophis' impact threat has disappeared, this asteroid remains an object of interest because of its close approach in 2029. The Earth encounter of Apophis in 2029 is expected to trigger varying degrees of alterations in the dynamics, spin-states, and surface arrangements of Apophis due to the Earth's gravitational perturbation (Yu et al. 2014; Souchay et al. 2014, 2018; DeMartini et al. 2019; Hirabayashi et al. 2021; Valvano

et al. 2022). Thus, the study of this asteroid will provide an excellent opportunity to examine the evolutionary process of its physical properties caused by planetary perturbation. For this reason, Apophis became a unique observation target and is the primary mission target of the Rendezvous Mission to Apophis, which is currently under pre-Phase A study in the Republic of Korea and scheduled for launch in 2027 (Moon et al. 2020).

The shape model and spin state are the most fundamental parameters for predicting the evolutionary process due to Earth's tidal effect. In addition, these properties provide important information for planning space mission scenarios. The spin state and convex shape model of Apophis were reconstructed using photometric data obtained from the 2012-2013 apparition (Pravec et al. 2014). They found it has non-principal axis (NPA) rotation in a short-axis mode (SAM) with rotation and precession periods of 263 and 27.38 hours, respectively, and the orientation of angular momentum vector of $\lambda_L = 250^\circ$ and $\beta_L = -75^\circ$. In addition, the convex shape model of Pravec et al. (2014) can be approximated by a prolate ellipsoid with a ratio of the greatest and intermediate principal moments of inertia (I_b/I_c) of 0.965, and the smallest principal moment of inertia (I_a/I_c) of 0.61.

For the last time before the 2029 Earth encounter, Apophis approached Earth on March 2021 at 0.11 AU and its apparent brightness increased to reach magnitude 16. Thus, the observation window for Apophis from the end of 2020 to the beginning of 2021 was the last opportunity to investigate its spin properties and refine the convex shape model. Therefore, we planned

Table 1. Details of the observatories and instruments in this campaign.

Telescope	Latitude	Longitude	Instrument
–Ground-based telescopes–			
Adiyaman Observatory 0.6 m	37:45:06 N	38:13:32 E	Andor Tech
AMU Winer, RBT 0.7m	31:39:56 N	110:36:06 W	Andor iXon
ATLAS HKO 0.5 m	20:42:27 N	156:15:25 W	STA-1600 10.5K CCD
ATLAS MLO 0.5 m	19:32:10 N	155:34:34 W	STA-1600 10.5K CCD
BOAO 1.8 m	36:09:53 N	128:58:36 E	E2V 4K CCD
CAHA 1.23 m	37:13:25 N	2:32:46 W	DLR MKIII camera
CAHA 2.2 m	37:13:25 N	2:32:46 W	CAFOS
DOAO 1.0 m	34:31:35 N	127:26:48 E	PI SOPHIA-2048B CCD
Kawabe Cosmic Park 1.0 m	33:53:27 N	135:13:12 E	FLI PL09000
KMTNet CTIO 1.6 m	30:10:02 S	70:48:14 W	18K mosaic CCD with four E2V 9K
KMTNet SAAO 1.6 m	32:22:43 S	20:48:37 E	18K mosaic CCD with four E2V 9K
KMTNet SSO 1.6 m	31:16:16 S	149:03:45 E	18K mosaic CCD with four E2V 9K
Krakow-CDK500 0.5 m	50:03:15 N	19:49:41 E	Apogee USB/Net
LCO CTIO A 1.0 m	30:10:03 S	70:48:17 W	Sinistro
LCO CTIO B 1.0 m	30:10:03 S	70:48:17 W	Sinistro
LCO McDonald A 1.0 m	30:41:47 S	104:00:54 E	Sinistro
LCO McDonald B 1.0 m	30:41:48 S	104:00:54 E	Sinistro
LCO SAAO A 1.0 m	32:23:50 N	20:48:37 W	Sinistro
LCO SAAO B 1.0 m	32:23:50 N	20:48:36 W	Sinistro
LCO SAAO C 1.0 m	32:23:51 N	20:48:36 W	Sinistro
LCO SSO A 1.0 m	31:16:22 N	149:04:14 W	Sinistro
LCO SSO B 1.0 m	31:16:23 N	149:04:15 W	Sinistro
LOAO 1.0 m	32:26:32 N	110:47:19 E	E2V 4K CCD
OWL Mitzpeh Ramon 0.5 m	30:35:51 N	34:45:48 E	FLI 16803
OWL Oukaimeden 0.5 m	31:12:21 N	7:52:00 W	FLI 16803
OWL Tucson 0.5 m	32:26:31 N	110:47:21 W	FLI 16803
OWL Yeongcheon 0.5 m	36:09:50 N	128:58:33 E	FLI 16803
SAAO Lesedi 1.0 m	32:22:47 S	20:48:36 E	SHOC (Andor iXon 888)
Skynet DSO-14, 0.4 m	36:15:01 N	81:24:45 W	Apogee USB/Net
Skynet Prompt5, 0.4 m	30:10:03 S	70:48:19 W	Apogee USB/Net
Skynet Prompt6, 0.4 m	30:10:03 S	70:48:19 W	FLI
Skynet Prompt MO 1 0.4 m	31:38:18 S	116:59:19 E	Apogee USB/Net
Skynet RRRT 0.6 m	37:52:44 N	78:41:39 W	SBIG STX-16803 3 CCD
SOAO 0.6 m	36:56:04 N	128:27:27 E	FLI 4K
Suhora Observatory Zeiss-60	49:34:09 N	20:04:03 E	Apogee AltaU-47
TUG 1.0 m	36:49:27 N	30:20:08 E	SI 4K
–Space-based telescope–			
TESS 0.1 m			four MIT Lincoln Lab. CCID-80 devices

Notes. AMU = Adam Mickiewicz University, RBT = Roman Baranowski Telescope, ATLAS = Asteroid Terrestrial-impact Last Alert System, HKO = Haleakala Observatory, MLO = Mauna Loa Observatory, BOAO = Bohyunsan Optical Astronomy Observatory, DOAO = Deokheung Optical Astronomy Observatory, CAHA = Calar Alto Observatory, KMTNet = Korea Microlensing Telescope (Kim et al. 2016), CTIO = Cerro Tololo Inter-American Observatory, SAAO = South African Astronomical Observatory, SSO = Siding Spring Observatory, LCO = Las Cumbres Observatory, LOAO = Lemonsan Optical Astronomy Observatory, CDK = Corrected Dall-Kirkham, OWL = Optical Wide-field patrol Network, DSO = Dark Sky Observatory, MO = Meckering Observatory, RRRT = Rapid Response Robotic Telescope, SOAO = Sobaeksan Optical Astronomy Observatory, TUG = TÜBİTAK National observatory, TESS = Transiting Exoplanet Survey Satellite, CAFOS = Calar Alto Faint Object Spectrograph

a photometric observation campaign for Apophis during this apparition. The details of our observation campaign are described in Section 2. In Section 3, a period analysis and reconstruction of the spin state and shape model of Apophis are reported. Finally, the summary and conclusions of this letter are given in Section 4.

2. Photometric observation campaign in the 2020-2021 apparition

As mentioned above, the 2020-2021 apparition of Apophis was the last opportunity to reveal the physical properties of this asteroid before its 2029 close approach. Therefore, we organized an

extensive and long-term photometric observation campaign for Apophis during this apparition. Our observation campaign was conducted by using not only the ground-based telescope but also the space telescope that is Transiting Exoplanet Survey Satellite (TESS; Ricker et al. 2015) spacecraft. The details of telescopes and instruments used in our campaign are provided in Table 1. The geometries and observational circumstances are listed in Table A.1. This campaign's data also contributed to the global Apophis Planetary Defense Campaign (Reddy et al. 2022).

Ground-based observations were carried out in 11 countries, including the Republic of Korea, the US, Chile, South Africa, Australia, Poland, Spain, Turkey, and Japan using 36 telescopes.

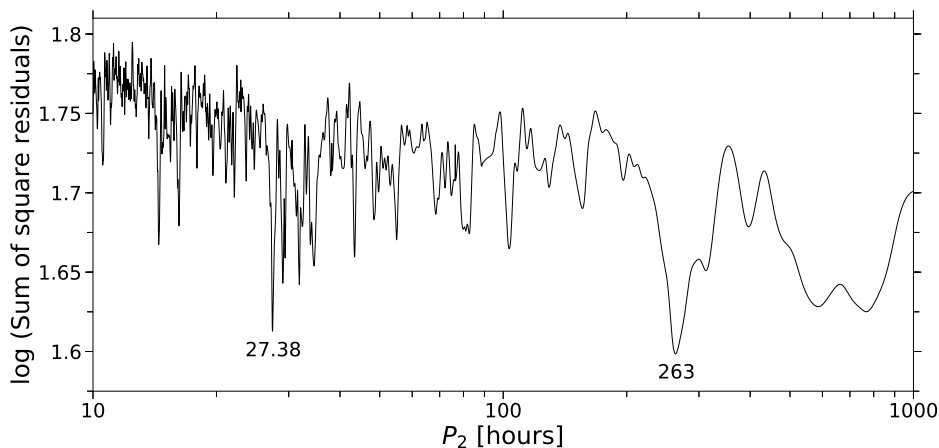


Fig. 1. P_2 search diagram of Apophis. The sum of square residuals were calculated for the 4-th order two-period Fourier series with $P_1 = 30.56$ hours fitted to our dense light curve obtained from 2021-02-07.0 to 2021-03-16.2 in flux units.

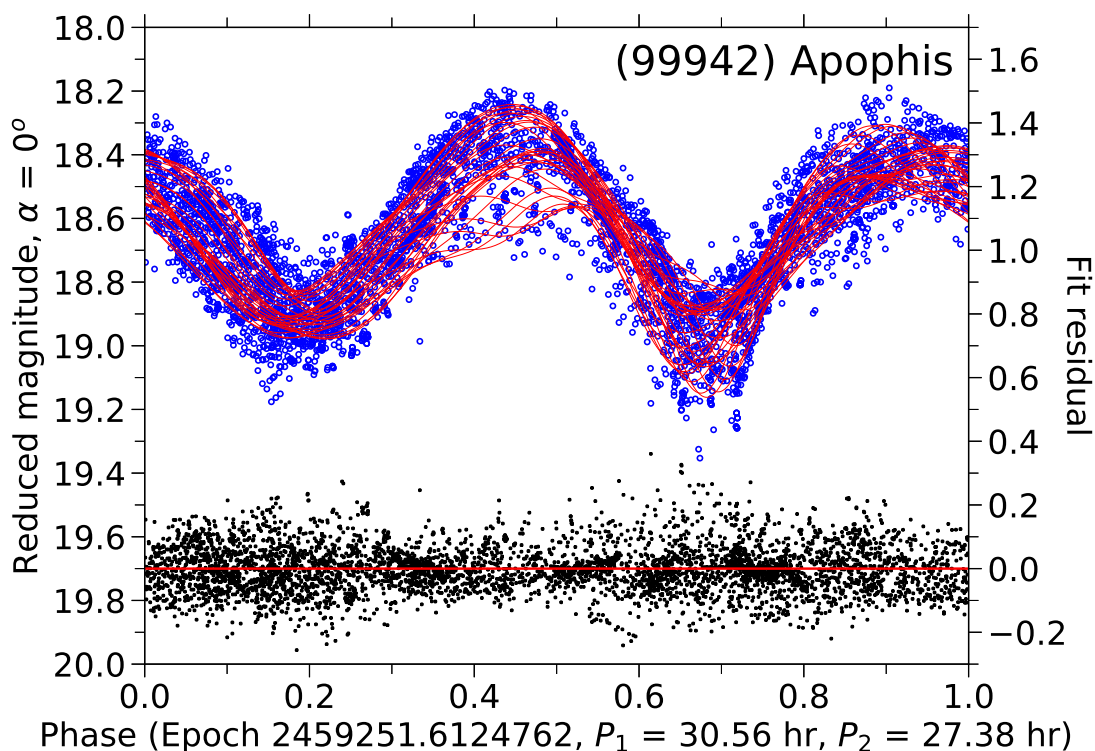


Fig. 2. The light curve of Apophis taken from 2021-02-07.0 to 2021-03-16.2 reduced to the unit geo- and heliocentric distance and to a consistent solar phase angle. The blue open circles indicate the photometric data folded with P_1 . The red curves denote the best-fit 4th order two-period Fourier series with the periods $P_1 = 30.56$ hours and $P_2 = 27.38$ hours. The black squares indicate the residuals of the photometric data from the 4th order two-period Fourier series (see the right ordinates).

Through our observation campaign, we observed 214 dense-in-time light curves and two sparse-in-time light curves. The dense-in-time light curves were obtained using a Johnson-Cousins V or R filter except for the data from the Kawabe Cosmic Park, which used the SDSS r' filter. As the observations were made with different telescopes and instruments, the data reduction processes may be slightly different. All data reductions were conducted following the standard manner. The bias- and flat-field images corrected, and the instrument magnitudes for each frame were measured using aperture photometry. All photometric data were calibrated with ATLAS Refcat2 (The ATLAS All-Sky Stellar

Reference Catalog; Tonry et al. 2018a). The magnitudes of ATLAS Refcat2 were converted to Johnson-Cousins V and R magnitudes using empirical transformation equations (Tonry et al. 2012). On the other hand, the sparse-in-time light curves were obtained from ATLAS (Tonry et al. 2018a,b). The ATLAS light curve was observed between November 2020 and April 2021 using orange (o , 560–820 nm) and cyan (c , 420–650 nm) filters.

We also gathered the long-term continuous photometric data observed from the TESS spacecraft using a wide I passband (see Figure 1 in Ricker et al. (2015)). TESS photometric data have been obtained in a similar manner as it was done in (Pál et al.

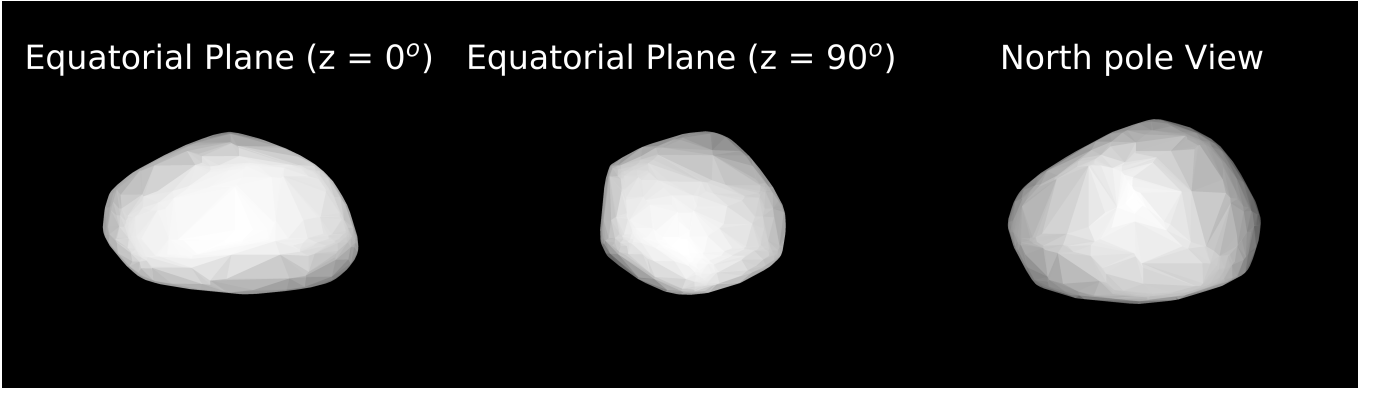


Fig. 3. Convex shape model of Apophis.

2020) for the image series of Sector 35 as acquired between 2021-02-19 and 2021-03-07. The individual photometric data points were derived using a convolution-based differential image analysis by employing the tools of the FITSH package Pál (2012).

3. Results

3.1. Periodic analysis

Before the shape model and spin state of Apophis were reconstructed, we performed periodic analysis of the light curve obtained from our observation campaign. To minimize the possible systematic effects caused by the changes in the observing geometry, this analysis was only conducted using the dense-in-time light curves observed with phase angles from 20° to 40° , which corresponds to the period from 2021-02-07.0 to 2021-03-16.2. Because our observations were made with different filters, we corrected them to match the R-filter using the color indices $V - R = 0.38$, $R - T = 0.07$, and $r' - R = 0.33$. The data were converted to flux units, and the helio- and geocentric distances were corrected to the unit distance and the solar phase angle to a consistent value using the H-G phase relation assuming $G = 0.24$. As Apophis exhibited tumbling motion, we attempted to detect double periods from the light curve of this asteroid.

First, the Lomb-Scargle method (Lomb 1976; Scargle 1982) was adopted to search for periodicities in the light curve. The strongest signal in the Lomb-Scargle periodogram was found at a period of 15.28 hours. The Lomb-Scargle method performs periodic analysis based on a single peak light curve. However, most light curves of asteroids have double peaks because their shapes are elongated. Therefore, we determined the primary period (P_1) on the light curve of Apophis as 30.56 hours that is double the strongest signal in the Lomb-Scargle periodogram.

The secondary period (P_2) was determined using the two-period Fourier series method (Pravec et al. 2005, 2014). The two-period Fourier series employed in this analysis are presented as follows:

$$F(t) = C_0 + \sum_{j=1}^m \left[C_{j0} \cos \frac{2\pi j}{P_1} t + S_{j0} \sin \frac{2\pi j}{P_1} t \right] + \sum_{k=1}^m \sum_{j=-m}^m \left[C_{jk} \cos \left(\frac{2\pi j}{P_1} + \frac{2\pi k}{P_2} \right) t + S_{jk} \sin \left(\frac{2\pi j}{P_1} + \frac{2\pi k}{P_2} \right) t \right]$$

The result for the P_2 search is shown in Figure 1, where the abscissa is P_2 and the ordinate is the sum of the squared resid-

Table 2. Parameters of the Apophis model.

	This Work	Pravec et al. (2014)
λ_L [deg]	278^{+9}_{-8}	250 ± 27
β_L [deg]	-86^{+5}_{-4}	-75 ± 14
P_ψ [hour]	264.18 ± 0.03	263 ± 6
P_ϕ [hour]	27.3855 ± 0.0003	27.38 ± 0.07
ψ_0^a [deg]	3^{+5}_{-1}	14^{+44}_{-11}
ϕ_0^a [deg]	183^{+7}_{-4}	152^{+173}_{-64}
I_a/I_c	$0.64^{+0.02}_{-0.09}$	$0.61^{+0.11}_{-0.08}$
I_b/I_c	$0.962^{+0.023}_{-0.002}$	$0.965^{+0.009}_{-0.015}$
$a_{\text{dyn}}/c_{\text{dyn}}$	1.48 ± 0.19	1.51 ± 0.18
$b_{\text{dyn}}/c_{\text{dyn}}$	1.06 ± 0.04	1.06 ± 0.02
$a_{\text{shape}}/c_{\text{shape}}$	1.56 ± 0.04	1.64 ± 0.09
$b_{\text{shape}}/c_{\text{shape}}$	1.12 ± 0.03	$1.14^{+0.04}_{-0.08}$
E/E_0	1.018 ± 0.010	1.024 ± 0.013

Notes. λ_L and β_L are the ecliptic coordinates of the constant angular momentum vector \mathbf{L} ; ψ_0 and ϕ_0 are the standard Euler angles at epoch JD₀; I_a , I_b and I_c are the dynamical moments of inertia corresponding to the longest-, intermediate-, and shortest-axes; $a_{\text{dyn}}/c_{\text{dyn}}$ and $c_{\text{dyn}}/c_{\text{dyn}}$ are the axial ratios of a dynamically equivalent ellipsoid; $a_{\text{shape}}/c_{\text{shape}}$ and $c_{\text{shape}}/c_{\text{shape}}$ are the axial ratios of a convex shape model; E/E_0 is the ratio of the rotational kinetic energy to the lowest energy for the given angular momentum.

^a The epoch JD₀ is 2456284.676388 (2012-12-23.176388).

uals for the fitted 4-th order two-period Fourier series with $P_1 = 30.56$ hours. From our P_2 search, we found two minimums at 27.38 and 263 hours. As the long period of 263 hours was a combination of the short period of 27.38 hours with P_1 , that is, $263^{-1} \approx 27.38^{-1} - 30.56^{-1}$, it seems to be derived from the short period. Thus, we determined P_2 as 27.38 hours. Figure 2 shows a composite light curve of Apophis obtained from 2021-02-07.0 to 2021-03-16.2 with the fitted 4-th order two-period Fourier series for periods 30.56 and 27.38 hours.

3.2. Reconstruction of the convex shape model and spin state from light curves

Given that the radar observation of Apophis suggested that it has a bifurcated shape (Brozović et al. 2018), the non-convex shape model may be a more suitable description of its actual shape. Nonetheless, this non-convex model obtained using photometric data should be applied only after very careful consideration. It is generally not possible to uniquely reconstruct a non-convex model using only photometric data (Viikinkoski et al. 2017; Har-

ris & Warner 2020). Further, concavities can be revealed only when reconstruction is performed using data observed at sufficiently high phase angles (Ďurech & Kaasalainen 2003). Unfortunately, we did not obtain sufficient data at high phase angles to create a non-convex model of Apophis. Therefore, our analysis was conducted based on the convex shape model.

The convex shape model and spin state of Apophis were reconstructed using the light curve inversion method for the NPA rotator (Kaasalainen & Torppa 2001; Kaasalainen et al. 2001; Kaasalainen 2001) combined with Hapke's light-scattering model (Hapke 1993). In this work, we used not only the light curves obtained through our campaign observation but also all available observation data collected from the literature. The historical light curves are listed in Table A.2.

The first step in revealing the spin state of a tumbling asteroid is to determine the physical periods, that is, the rotation (P_ψ) and precession period (P_ϕ). Because the periods on the light curve were derived from the physical periods, P_1^{-1} and P_2^{-1} usually appear at P_ϕ^{-1} and $P_\phi^{-1} \pm P_\psi^{-1}$, where the plus sign is for the long-axis mode (LAM) and the minus sign for SAM (Kaasalainen 2001). Therefore, we found two possible physical period combinations using the period obtained in the previous section: $P_1^{-1} = P_\phi^{-1}$ and $P_2^{-1} = P_\phi^{-1} + P_\psi^{-1}$ (LAM); $P_1^{-1} = P_\phi^{-1} - P_\psi^{-1}$ and $P_2^{-1} = P_\phi^{-1}$ (SAM). The optimization for each P_ϕ was performed in the same way as in Lee et al. (2020, 2021). In these produces, the Hapke's model parameters were set to a typical S-type asteroid's: $\varpi = 0.23$, $g = -0.27$, $h = 0.08$, $B_0 = 1.6$, and $\bar{\theta} = 20^\circ$ (Li et al. 2015). Because we did not obtain the data observed at low solar phase angles, the parameters for the opposition surge, h and B_0 , and the roughness $\bar{\theta}$ were fixed. Only the ϖ and g parameters were optimized. It was found that the inertia tensor of the convex shape model for the LAM solution was not consistent with the kinematic I_1 and I_2 parameters. Therefore, we decided to use SAM as the final solution.

The best-fit model for Apophis is listed in Table 2, together with Pravec et al. (2014) solution for comparison. Further, the uncertainties of our model parameters corresponded to a 3σ confidence interval. The confidence interval was estimated from the increase in the χ^2 value when the solved-for physical parameters were varied. The threshold corresponding to the 3σ confidence interval was set as $\chi_{min}^2 \times (1 + 3\sqrt{2/\nu})^1$, where the χ_{min}^2 represents the χ^2 value for the best-fit solution and ν represents the number of degrees of freedom (Vokrouhlický et al. 2017). The convex shape model of Apophis is shown in Figure 3. The synthetic light curve of our model and the observed light curve are presented in Appendix B.

4. Summary and Conclusions

In this letter, we present the convex shape model and spin state of Apophis reconstructed using historical and newly obtained light curves. The new photometric data were observed from an extensive and long-term photometric observation campaign for Apophis during its 2020–2021 apparition using 36 facilities, including the ground-based and space telescope. We obtained 211 dense-in-time light curves and two sparse-in-time light curves. In the period analysis conducted with our dense light curve, double periods were detected as 30.56 and 27.38 hours, respectively.

The best-fit solution indicates that Apophis is in a SAM state with rotation and precession periods of 264.178 ± 0.01 and

27.38547 ± 0.00002 hours, respectively. The ecliptic coordinates of the angular momentum vector orientation of this asteroid are $(275 \pm 3^\circ, -85 \pm 1^\circ)$. In addition, the ratio of the dynamical moments of inertia was estimated as $I_a/I_c = 0.64$ and $I_b/I_c = 0.96$. Our model was similar to that of Pravec et al. (2014). Nonetheless, the uncertainties of the model parameters were improved because they were reconstructed based on the dataset obtained from the two apparitions. This model will be useful not only for investigating changes in Apophis' physical properties due to the tidal effect during its encounter in 2029 but also for planning a space mission to this asteroid.

Acknowledgements. This research has made use of the KMTNet system operated by the Korea Astronomy and Space Science Institute (KASI) and the data were obtained at three host sites of CTIO in Chile, SAAO in South Africa, and SSO in Australia. This paper was partially based on observations obtained at the Bohyunsan Optical Astronomy Observatory (BOAO), the Sobaeksan Optical Astronomy Observatory (SOAO), and the Lemmonsan Optical Astronomy Observatory (LOAO), which is operated by the Korea Astronomy and Space Science Institute (KASI). This work has made use of data from the Asteroid Terrestrial-impact Last Alert System (ATLAS) project. The Asteroid Terrestrial-impact Last Alert System (ATLAS) project is primarily funded to search for near earth asteroids through NASA grants NN12AR55G, 80NSSC18K0284, and 80NSSC18K1575; byproducts of the NEO search include images and catalogs from the survey area. The ATLAS science products have been made possible through the contributions of the University of Hawaii Institute for Astronomy, the Queen's University Belfast, the Space Telescope Science Institute, the South African Astronomical Observatory, and The Millennium Institute of Astrophysics (MAS), Chile. A.P. and R.S. were supported by the K-138962 grant of the National Research, Development and Innovation Office. R.D. acknowledge financial support from the State Agency for Research of the Spanish MCIU through the "Center of Excellence Severo Ochoa" award for the Instituto de Astrofísica de Andalucía (SEV-2017-0709). Based on observations collected at Centro Astronómico Hispano en Andalucía (CAHA) at Calar Alto, operated jointly by Instituto de Astrofísica de Andalucía (CSIC) and Junta de Andalucía.

References

- Binzel, R. P., Rivkin, A. S., Thomas, C. A., et al. 2009, *Icarus*, 200, 480
 Brozović, M., Benner, L. A. M., McMichael, J. G., et al. 2018, *Icarus*, 300, 115
 Chesley, S. R. 2006, in *Asteroids, Comets, Meteors*, ed. D. Lazzaro, S. Ferraz-Mello, & J. A. Fernández, Vol. 229, 215–228
 DeMartini, J. V., Richardson, D. C., Barnouin, O. S., et al. 2019, *Icarus*, 328, 93
 Giorgini, J. D., Benner, L. A. M., Ostro, S. J., Nolan, M. C., & Busch, M. W. 2008, *Icarus*, 193, 1
 Greicius, T. 2021, NASA Analysis: Earth Is Safe From Asteroid Apophis for 100-Plus Years, accessed:26-Mar-2021
 Hapke, B. 1993, *Theory of reflectance and emittance spectroscopy* (Cambridge: Cambridge University Press)
 Harris, A. & Warner, B. D. 2020, *Icarus*, 339, 113602
 Hirabayashi, M., Kim, Y., & Brozović, M. 2021, *Icarus*, 365, 114493
 Kaasalainen, M. 2001, *A&A*, 376, 302
 Kaasalainen, M. & Torppa, J. 2001, *Icarus*, 153, 24
 Kaasalainen, M., Torppa, J., & Muinonen, K. 2001, *Icarus*, 153, 37
 Kim, S.-L., Lee, C.-U., Park, B.-G., et al. 2016, *Journal of Korean Astronomical Society*, 49, 37
 Lee, H. J., Ďurech, J., Kim, M. J., et al. 2020, *A&A*, 635, A137
 Lee, H.-J., Ďurech, J., Vokrouhlický, D., et al. 2021, *AJ*, 161, 112
 Li, J. Y., Helfenstein, P., Buratti, B., Takir, D., & Clark, B. E. 2015, in *Asteroids IV*, ed. P. Michel, F. E. DeMeo, & W. F. Bottke (Tucson: University of Arizona Press), 129–150
 Lomb, N. R. 1976, *Ap&SS*, 39, 447
 Moon, H. K., Choi, Y. J., Kim, M. J., et al. 2020, in *LPI Contributions*, Vol. 2242, Apophis T-9 Years: Knowledge Opportunities for the Science of Planetary Defense, 2065
 Pál, A. 2012, *MNRAS*, 421, 1825
 Pál, A., Szakáts, R., Kiss, C., et al. 2020, *ApJS*, 247, 26
 Pravec, P., Harris, A. W., Scheirich, P., et al. 2005, *Icarus*, 173, 108
 Pravec, P., Scheirich, P., Ďurech, J., et al. 2014, *Icarus*, 233, 48
 Reddy, V., Kelley, M. S., Dotson, J., et al. 2022, submitted
 Reddy, V., Sanchez, J. A., Furfaro, R., et al. 2018, *AJ*, 155, 140
 Ricker, G. R., Winn, J. N., Vanderspek, R., et al. 2015, *Journal of Astronomical Telescopes, Instruments, and Systems*, 1, 014003
 Scargle, J. D. 1982, *ApJ*, 263, 835
 Souchay, J., Lhotka, C., Heron, G., et al. 2018, *A&A*, 617, A74

¹ These was a typo in Vokrouhlický et al. (2017), so we used $2/\nu$ instead of 2ν .

- Souchay, J., Souami, D., Lhotka, C., Puente, V., & Folgueira, M. 2014, *A&A*, 563, A24
- Tonry, J. L., Denneau, L., Flewelling, H., et al. 2018a, *ApJ*, 867, 105
- Tonry, J. L., Denneau, L., Heinze, A. N., et al. 2018b, *PASP*, 130, 064505
- Tonry, J. L., Stubbs, C. W., Lykke, K. R., et al. 2012, *ApJ*, 750, 99
- Valvano, G., Winter, O. C., Sfair, R., et al. 2022, *MNRAS*, 510, 95
- Đurech, J. & Kaasalainen, M. 2003, *A&A*, 404, 709
- Viikinkoski, M., Hanuš, J., Kaasalainen, M., Marchis, F., & Ďurech, J. 2017, *A&A*, 607, A117
- Vokrouhlický, D., Pravec, P., Ďurech, J., et al. 2017, *AJ*, 153, 270
- Warner, B. D. & Stephens, R. D. 2021, *Minor Planet Bulletin*, 48, 294
- Yu, Y., Richardson, D. C., Michel, P., Schwartz, S. R., & Ballouz, R.-L. 2014, *Icarus*, 242, 82

-
- ¹ Korea Astronomy and Space Science Institute, 776, Daedeokdae-ro, Yuseong-gu, Daejeon 34055, Korea
e-mail: hjlee@kasi.re.kr
- ² Astronomical Observatory Institute, Faculty of Physics, A. Mickiewicz University, Słoneczna 36, 60-286 Poznań, Poland
- ³ Chungbuk National University, 1 Chungdae-ro, Seowon-gu, Cheongju, Chungbuk 28644, Korea
- ⁴ University of Science and Technology, 217, Gajeong-ro, Yuseong-gu, Daejeon 34113, Korea
- ⁵ Astronomical Observatory, Jagiellonian University, ul. Orla 171, 30-244 Kraków, Poland
- ⁶ Mt. Suhora Observatory, Pedagogical University, ul. Pochorążych 2, 30-084 Kraków, Poland
- ⁷ Las Cumbres Observatory, 6740 Cortona Drive Suite 102, Goleta, CA 93117, USA
- ⁸ Las Cumbres Observatory, School of Physics and Astronomy, Cardiff University, QueensBuildings, The Parade, Cardiff CF24 3AA, UK
- ⁹ Asteroid Institute, 20 Sunnyside Ave, Suite 427, Mill Valley, CA 94941, USA
- ¹⁰ Department of Astronomy and the DIRAC Institute, University of Washington, 3910 15thAve NE, Seattle, WA 98195, USA
- ¹¹ Konkoly Observatory, Research Centre for Astronomy and Earth Sciences, Eötvös Loránd Research Network (ELKH), H-1121 Budapest, Konkoly Thege Miklós út 15-17, Hungary
- ¹² South African Astronomical Observatory, Cape Town, 7925, South Africa
- ¹³ Department of Astronomy, University of Cape Town, Rondebosch, 7701, South Africa
- ¹⁴ Kepler Institute of Astronomy, University of Zielona Góra, Lubuska 2, 65-265 Zielona Góra, Poland
- ¹⁵ Departamento de Sistema Solar, Instituto de Astrofísica de Andalucía (CSIC), Glorieta de la Astronomía s/n, 18008 Granada, Spain
- ¹⁶ National Youth Space Center, Goheung, Jeollanam-do 59567, Korea
- ¹⁷ Deutsches Zentrum für Luft- und Raumfahrt (DLR), Institute of Planetary Research, D-12489 Berlin, Germany
- ¹⁸ University of Occupational and Environmental Health, Japan, 1-1 Iseigaoka, Yahata, Kitakyusyu 807-8555, Japan
- ¹⁹ Planetary Exploration Research Center, Chiba Institute of Technology, 2-17-1 Tsudanuma, Narashino, Chiba, 275-0016, Japan
- ²⁰ University of North Carolina at Chapel Hill, Chapel Hill, North Carolina NC 27599, USA
- ²¹ Department of Physics, Adiyaman University, 02040 Adiyaman, Turkey
- ²² Dark Sky Observatory, Dept. of Physics and Astronomy, Appalachian State University, Boone, NC 28608, USA
- ²³ Akdeniz University, Department of Space Sciences and Technologies, 07058 Antalya, Turkey
- ²⁴ TÜBİTAK National Observatory, Akdeniz University Campus, 07058 Antalya, Turkey

Appendix A: Additional tables

Table A.1. The geometries and observational circumstances.

Date UT	R. A. (h m)	Dec. (° ′)	r_h (AU)	Δ (AU)	α (°)	Observatory	Filter
--Dense photometry--							
2021-01-16.5	11 44	-17 26	1.076	0.203	58.2	LOAO	R
2021-01-17.5	11 43	-17 37	1.077	0.200	57.5	LOAO	R
2021-01-18.5	11 43	-17 48	1.078	0.198	56.7	LOAO	R
2021-01-29.1	11 34	-19 16	1.091	0.170	48.1	SAAO Lesedi	VR
2021-02-05.0	11 21	-19 33	1.096	0.153	41.4	SAAO Lesedi	V
2021-02-05.4	11 20	-19 33	1.096	0.152	41.0	Skynet Prompt5	R
2021-02-06.0	11 19	-19 31	1.096	0.151	40.3	SAAO Lesedi	V
2021-02-06.3	11 18	-19 31	1.096	0.150	40.0	OWL USA	R
2021-02-07.0	11 16	-19 29	1.097	0.148	39.3	CAHA 2.2 m	R
2021-02-07.1	11 16	-19 28	1.097	0.148	39.2	LCO SAAO A	R
2021-02-07.1	11 16	-19 28	1.097	0.148	39.2	LCO SAAO B	R
2021-02-07.1	11 16	-19 28	1.097	0.148	39.2	SAAO Lesedi	V
2021-02-07.2	11 16	-19 28	1.097	0.148	39.1	LCO CTIO A	R
2021-02-07.3	11 15	-19 28	1.097	0.148	38.9	OWL USA	R
2021-02-07.3	11 15	-19 28	1.097	0.148	38.9	Skynet Prompt5	R
2021-02-07.8	11 14	-19 26	1.097	0.147	38.4	LCO SAAO C	R
2021-02-08.0	11 14	-19 25	1.097	0.146	38.2	LCO SAAO A	R
2021-02-08.0	11 14	-19 25	1.097	0.146	38.2	LCO SAAO B	R
2021-02-08.1	11 13	-19 24	1.097	0.146	38.1	SAAO Lesedi	V
2021-02-08.3	11 13	-19 23	1.097	0.145	37.8	LCO CTIO A	R
2021-02-08.3	11 13	-19 23	1.097	0.145	37.8	LCO McDonald A	R
2021-02-08.3	11 13	-19 23	1.097	0.145	37.8	OWL USA	R
2021-02-08.3	11 13	-19 23	1.097	0.145	37.8	Skynet Prompt5	R
2021-02-08.6	11 12	-19 22	1.097	0.145	37.5	LCO SSO B	R
2021-02-08.9	11 11	-19 20	1.098	0.144	37.2	LCO SAAO A	R
2021-02-09.1	11 10	-19 19	1.098	0.144	37.0	LCO SAAO B	R
2021-02-09.1	11 10	-19 19	1.098	0.144	37.0	SAAO Lesedi	V
2021-02-09.3	11 10	-19 17	1.098	0.143	36.7	LCO McDonald B	R
2021-02-09.3	11 10	-19 17	1.098	0.143	36.7	Skynet Prompt5	R
2021-02-09.4	11 10	-19 17	1.098	0.143	36.6	OWL USA	R
2021-02-09.6	11 09	-19 15	1.098	0.142	36.4	LCO SSO B	R
2021-02-09.9	11 08	-19 13	1.098	0.142	36.1	LCO SAAO C	R
2021-02-10.0	11 08	-19 12	1.098	0.142	35.9	LCO SAAO A	R
2021-02-10.1	11 07	-19 12	1.098	0.141	35.8	LCO SAAO B	R
2021-02-10.1	11 07	-19 12	1.098	0.141	35.8	OWL MAR	R
2021-02-10.1	11 07	-19 12	1.098	0.141	35.8	SAAO Lesedi	V
2021-02-10.2	11 07	-19 11	1.098	0.141	35.7	Skynet Prompt5	R
2021-02-10.3	11 07	-19 10	1.098	0.141	35.6	LCO CTIO B	R
2021-02-10.4	11 07	-19 09	1.098	0.141	35.5	LCO McDonald B	R
2021-02-10.5	11 06	-19 08	1.098	0.140	35.4	LCO SSO B	R
2021-02-11.0	11 05	-19 04	1.098	0.139	34.8	Adiyaman Observatory	R
2021-02-11.0	11 05	-19 04	1.098	0.139	34.8	LCO SAAO C	R
2021-02-11.0	11 05	-19 04	1.098	0.139	34.8	OWL ISR	R
2021-02-11.1	11 04	-19 03	1.098	0.139	34.7	OWL MAR	R
2021-02-11.2	11 04	-19 02	1.098	0.139	34.6	LCO CTIO A	R
2021-02-11.3	11 04	-19 01	1.098	0.139	34.5	LCO CTIO B	R
2021-02-11.3	11 04	-19 01	1.098	0.139	34.5	Skynet Prompt5	R
2021-02-11.4	11 03	-19 00	1.098	0.139	34.3	Winer Observatory RBT	R
2021-02-11.5	11 03	-18 59	1.098	0.138	34.2	LCO SSO A	R
2021-02-11.5	11 03	-18 59	1.098	0.138	34.2	OWL USA	R
2021-02-12.0	11 01	-18 54	1.099	0.137	33.7	Adiyaman Observatory	R
2021-02-12.2	11 01	-18 52	1.099	0.137	33.4	OWL MAR	R
2021-02-12.3	11 00	-18 51	1.099	0.137	33.3	Winer Observatory RBT	R
2021-02-12.4	11 00	-18 50	1.099	0.136	33.2	OWL USA	R
2021-02-12.7	10 59	-18 46	1.099	0.136	32.9	Skynet Prompt MO1	R
2021-02-13.2	10 57	-18 40	1.099	0.135	32.3	Skynet Prompt5	R

Table A.1. continued.

Date UT	R. A. (h m)	Dec. (° ')	r_h (AU)	Δ (AU)	α (°)	Observatory	Filter
2021-02-14.0	10 54	-18 29	1.099	0.133	31.4	Adiyaman Observatory	R
2021-02-15.1	10 50	-18 13	1.099	0.131	30.1	CAHA 2.2 m	R
2021-02-16.1	10 47	-17 55	1.099	0.129	29.0	OWL MAR	R
2021-02-16.4	10 45	-17 50	1.099	0.129	28.6	Skynet Prompt5	R
2021-02-16.6	10 45	-17 46	1.099	0.128	28.4	Skynet Prompt MO1	R
2021-02-16.9	10 43	-17 40	1.099	0.128	28.1	OWL MAR	R
2021-02-17.4	10 41	-17 30	1.099	0.127	27.5	Winer Observatory RBT	R
2021-02-17.7	10 40	-17 24	1.099	0.127	27.2	Skynet Prompt MO1	R
2021-02-18.4	10 37	-17 09	1.099	0.125	26.5	LOAO	R
2021-02-18.4	10 37	-17 09	1.099	0.125	26.5	Winer Observatory RBT	R
2021-02-18.7	10 36	-17 02	1.099	0.125	26.1	SOAO	R
2021-02-18.8	10 36	-16 60	1.099	0.125	26.0	Skynet Prompt MO1	R
2021-02-19.0	10 35	-16 55	1.099	0.125	25.8	Suhora Observatory	R
2021-02-19.3	10 34	-16 48	1.099	0.124	25.5	LOAO	R
2021-02-19.3	10 34	-16 48	1.099	0.124	25.5	Winer Observatory RBT	R
2021-02-19.6	10 32	-16 40	1.099	0.124	25.2	BOAO	R
2021-02-19.6	10 32	-16 40	1.099	0.124	25.2	OWL KOR	R
2021-02-19.6	10 32	-16 40	1.099	0.124	25.2	SOAO	R
2021-02-19.7	10 32	-16 38	1.099	0.123	25.2	Skynet Prompt MO1	R
2021-02-20.3	10 29	-16 23	1.099	0.123	24.6	LOAO	R
2021-02-20.5	10 28	-16 17	1.099	0.122	24.4	Skynet Prompt MO1	R
2021-02-20.6	10 28	-16 15	1.099	0.122	24.3	BOAO	R
2021-02-21.0	10 26	-16 04	1.099	0.122	24.0	Suhora Observatory	R
2021-02-21.4	10 25	-15 52	1.099	0.121	23.6	Winer Observatory RBT	R
2021-02-21.6	10 24	-15 47	1.099	0.121	23.5	BOAO	R
2021-02-21.8	10 23	-15 41	1.099	0.121	23.3	OWL ISR	R
2021-02-22.5	10 20	-15 20	1.099	0.120	22.8	Skynet Prompt MO1	R
2021-02-22.7	10 19	-15 14	1.098	0.119	22.6	BOAO	R
2021-02-22.7	10 19	-15 14	1.098	0.119	22.6	Skynet Prompt MO1	R
2021-02-23.1	10 17	-15 01	1.098	0.119	22.4	OWL USA	R
2021-02-24.2	10 12	-14 25	1.098	0.118	21.8	OWL USA	R
2021-02-25.0	10 08	-13 58	1.098	0.117	21.4	Suhora Observatory	R
2021-02-26.2	10 03	-13 14	1.097	0.116	21.1	OWL USA	R
2021-02-27.2	09 58	-12 36	1.097	0.115	21.1	OWL USA	R
2021-02-28.0	09 54	-12 04	1.096	0.115	21.2	CAHA 2.2 m	R
2021-02-28.0	09 54	-12 04	1.096	0.115	21.2	Skynet Prompt5	R
2021-03-01.2	09 49	-11 14	1.096	0.114	21.5	OWL USA	R
2021-03-01.9	09 45	-10 45	1.095	0.114	21.9	TUG	R
2021-03-03.0	09 40	-09 57	1.095	0.113	22.6	OWL MAR	R
2021-03-03.0	09 40	-09 57	1.095	0.113	22.6	Suhora Observatory	R
2021-03-03.0	09 40	-09 57	1.095	0.113	22.6	KMTNet CTIO	VR
2021-03-03.0	09 40	-09 57	1.095	0.113	22.6	Skynet Prompt5	R
2021-03-03.2	09 39	-09 48	1.095	0.113	22.7	OWL USA	R
2021-03-03.2	09 39	-09 48	1.095	0.113	22.7	Winer Observatory RBT	R
2021-03-03.4	09 39	-09 39	1.095	0.113	22.9	KMTNet SSO	VR
2021-03-05.1	09 31	-08 21	1.093	0.113	24.4	LCO CTIO A	R
2021-03-05.2	09 30	-08 16	1.093	0.113	24.5	LCO McDonald A	R
2021-03-05.4	09 30	-08 07	1.093	0.113	24.7	LCO SSO B	R
2021-03-05.6	09 29	-07 58	1.093	0.113	24.9	LCO SSO A	R
2021-03-05.8	09 28	-07 48	1.093	0.113	25.1	LCO SAAO A	R
2021-03-05.8	09 28	-07 48	1.093	0.113	25.1	LCO SAAO C	R
2021-03-06.4	09 25	-07 20	1.092	0.113	25.8	LCO SSO B	R
2021-03-06.5	09 25	-07 15	1.092	0.113	25.9	LCO SSO A	R
2021-03-06.8	09 23	-07 01	1.092	0.113	26.3	LCO SAAO C	R
2021-03-06.8	09 23	-07 01	1.092	0.113	26.3	OWL ISR	R
2021-03-06.9	09 23	-06 56	1.092	0.113	26.4	LCO SAAO A	R
2021-03-06.9	09 23	-06 56	1.092	0.113	26.4	OAUJ CDK500	R
2021-03-07.0	09 22	-06 51	1.092	0.113	26.5	LCO CTIO B	R
2021-03-07.1	09 22	-06 47	1.092	0.113	26.6	OWL USA	R
2021-03-07.2	09 22	-06 42	1.092	0.113	26.8	LCO McDonald A	R

Table A.1. continued.

Date UT	R. A. (h m)	Dec. (° ')	r_h (AU)	Δ (AU)	α (°)	Observatory	Filter
2021-03-07.3	09 21	-06 37	1.092	0.113	26.9	LCO McDonald B	R
2021-03-07.4	09 21	-06 32	1.092	0.113	27.0	KMTNet SSO	VR
2021-03-07.5	09 20	-06 27	1.091	0.113	27.1	LCO SSO A	R
2021-03-07.6	09 20	-06 23	1.091	0.113	27.3	LCO SSO B	R
2021-03-07.8	09 19	-06 13	1.091	0.113	27.5	KMTNet SAAO	VR
2021-03-07.8	09 19	-06 13	1.091	0.113	27.5	LCO SAAO A	R
2021-03-07.9	09 19	-06 08	1.091	0.113	27.6	LCO SAAO C	R
2021-03-08.0	09 18	-06 03	1.091	0.113	27.8	LCO CTIO B	R
2021-03-08.1	09 18	-05 58	1.091	0.113	27.9	LCO McDonald A	R
2021-03-08.2	09 17	-05 54	1.091	0.113	28.0	LCO McDonald B	R
2021-03-08.8	09 15	-05 25	1.090	0.113	28.8	OWL ISR	R
2021-03-08.9	09 14	-05 20	1.090	0.113	29.0	LCO SAAO C	R
2021-03-09.0	09 14	-05 15	1.090	0.113	29.1	LCO CTIO B	R
2021-03-09.0	09 14	-05 15	1.090	0.113	29.1	LCO SAAO B	R
2021-03-09.5	09 12	-04 51	1.090	0.113	29.8	LCO SSO A	R
2021-03-09.6	09 12	-04 46	1.090	0.113	29.9	LCO SSO B	R
2021-03-09.6	09 12	-04 46	1.090	0.113	29.9	SOAO	R
2021-03-09.8	09 11	-04 36	1.089	0.113	30.2	KMTNet SAAO	VR
2021-03-09.8	09 11	-04 36	1.089	0.113	30.2	LCO SAAO B	R
2021-03-10.0	09 10	-04 26	1.089	0.113	30.5	Suhora Observatory	R
2021-03-10.2	09 09	-04 16	1.089	0.114	30.8	LCO CTIO A	R
2021-03-10.2	09 09	-04 16	1.089	0.114	30.8	Skynet DSO-14	R
2021-03-10.3	09 09	-04 12	1.089	0.114	30.9	OWL USA	R
2021-03-10.3	09 09	-04 12	1.089	0.114	30.9	Skynet RRRT	R
2021-03-10.3	09 09	-04 12	1.089	0.114	30.9	Winer Observatory RBT	R
2021-03-10.5	09 08	-04 02	1.089	0.114	31.2	BOAO	R
2021-03-10.5	09 08	-04 02	1.089	0.114	31.2	DOAO	R
2021-03-10.6	09 08	-03 57	1.089	0.114	31.3	SOAO	R
2021-03-10.6	09 08	-03 57	1.089	0.114	31.3	Kawabe Observatory	r'
2021-03-10.9	09 06	-03 42	1.088	0.114	31.8	CAHA 1.23 m	R
2021-03-10.9	09 06	-03 42	1.088	0.114	31.8	OAUJ CDK500	R
2021-03-11.0	09 06	-03 37	1.088	0.114	31.9	Suhora Observatory	R
2021-03-11.1	09 06	-03 33	1.088	0.114	32.1	LCO CTIO B	R
2021-03-11.2	09 05	-03 28	1.088	0.114	32.2	Skynet RRRT	R
2021-03-11.3	09 05	-03 23	1.088	0.114	32.4	OWL USA	R
2021-03-11.3	09 05	-03 23	1.088	0.114	32.4	Winer Observatory RBT	R
2021-03-11.8	09 03	-02 59	1.087	0.114	33.1	LCO SAAO A	R
2021-03-11.9	09 02	-02 54	1.087	0.114	33.2	LCO SAAO B	R
2021-03-11.9	09 02	-02 54	1.087	0.114	33.2	LCO SAAO C	R
2021-03-12.0	09 02	-02 49	1.087	0.114	33.4	LCO CTIO B	R
2021-03-12.2	09 01	-02 39	1.087	0.115	33.7	LCO CTIO A	R
2021-03-12.3	09 01	-02 34	1.087	0.115	33.8	Winer Observatory RBT	R
2021-03-12.6	08 60	-02 20	1.086	0.115	34.3	LCO SSO A	R
2021-03-12.7	08 60	-02 15	1.086	0.115	34.4	LCO SAAO B	R
2021-03-12.9	08 59	-02 05	1.086	0.115	34.7	LCO SAAO A	R
2021-03-12.9	08 59	-02 05	1.086	0.115	34.7	OAUJ CDK500	R
2021-03-12.9	08 59	-02 05	1.086	0.115	34.7	Suhora Observatory	R
2021-03-13.2	08 58	-01 51	1.086	0.115	35.2	LCO CTIO B	R
2021-03-13.6	08 56	-01 36	1.086	0.115	35.6	DOAO	R
2021-03-13.8	08 56	-01 22	1.085	0.116	36.1	TUG	R
2021-03-13.9	08 55	-01 17	1.085	0.116	36.2	LCO SAAO A	R
2021-03-14.0	08 55	-01 12	1.085	0.116	36.4	Skynet Prompt5	R
2021-03-14.0	08 55	-01 12	1.085	0.116	36.4	Skynet RRRT	R
2021-03-14.1	08 54	-01 07	1.085	0.116	36.5	LCO CTIO B	R
2021-03-14.3	08 54	+00 58	1.085	0.116	36.8	LCO McDonald A	R
2021-03-14.5	08 53	+00 48	1.084	0.116	37.1	BOAO	R
2021-03-15.0	08 51	+00 25	1.084	0.116	37.9	OAUJ CDK500	R
2021-03-15.0	08 51	+00 25	1.084	0.116	37.9	Skynet Prompt5	R
2021-03-15.1	08 51	+00 20	1.084	0.117	38.0	Skynet Prompt6	R
2021-03-15.1	08 51	+00 20	1.084	0.117	38.0	Skynet RRRT	R

Table A.1. continued.

Date UT	R. A. (h m)	Dec. (° ′)	r_h (AU)	Δ (AU)	α (°)	Observatory	Filter
2021-03-15.2	08 51	+00 15	1.084	0.117	38.2	LOAO	<i>R</i>
2021-03-15.9	08 48	+00 18	1.083	0.117	39.3	OAUJ CDK500	<i>R</i>
2021-03-16.0	08 48	+00 22	1.083	0.117	39.4	CAHA 2.2 m	<i>R</i>
2021-03-16.2	08 47	+00 32	1.082	0.118	39.7	LOAO	<i>R</i>
2021-03-16.6	08 46	+00 50	1.082	0.118	40.3	BOAO	<i>R</i>
2021-03-16.6	08 46	+00 50	1.082	0.118	40.3	DOAO	<i>R</i>
2021-03-16.9	08 45	+01 04	1.081	0.118	40.8	Adiyaman Observatory	<i>R</i>
2021-03-17.0	08 45	+01 09	1.081	0.118	40.9	CAHA 2.2 m	<i>R</i>
2021-03-17.0	08 45	+01 09	1.081	0.118	40.9	Skynet Prompt5	<i>R</i>
2021-03-17.1	08 45	+01 13	1.081	0.118	41.1	Skynet Prompt6	<i>R</i>
2021-03-17.6	08 43	+01 32	1.081	0.119	41.7	DOAO	<i>R</i>
2021-03-18.0	08 42	+01 55	1.080	0.119	42.4	CAHA 2.2 m	<i>R</i>
2021-03-18.2	08 41	+02 04	1.080	0.119	42.7	OWL USA	<i>R</i>
2021-03-18.4	08 41	+02 13	1.079	0.120	43.0	KMTNet SSO	<i>VR</i>
2021-03-18.8	08 40	+02 31	1.079	0.120	43.6	KMTNet SAAO	<i>VR</i>
2021-03-18.8	08 40	+02 31	1.079	0.120	43.6	OWL ISR	<i>R</i>
2021-03-19.2	08 38	+02 48	1.078	0.120	44.2	OWL USA	<i>R</i>
2021-03-19.9	08 37	+03 19	1.077	0.121	45.2	OWL ISR	<i>R</i>
2021-03-20.2	08 36	+03 32	1.077	0.122	45.7	OWL USA	<i>R</i>
2021-03-20.2	08 36	+03 32	1.077	0.122	45.7	Skynet RRRT	<i>R</i>
2021-03-21.2	08 33	+04 15	1.076	0.123	47.1	OWL USA	<i>R</i>
2021-03-22.3	08 30	+05 01	1.074	0.124	48.7	OWL USA	<i>R</i>
2021-03-22.5	08 30	+05 10	1.074	0.124	49.0	DOAO	<i>R</i>
2021-03-22.8	08 29	+05 22	1.073	0.125	49.4	KMTNet SAAO	<i>VR</i>
2021-03-24.8	08 25	+06 42	1.070	0.127	52.2	KMTNet SAAO	<i>VR</i>
2021-03-30.0	08 16	+09 53	1.061	0.134	59.0	KMTNet CTIO	<i>VR</i>
2021-03-30.7	08 15	+10 16	1.060	0.135	59.9	KMTNet SAAO	<i>VR</i>
2021-04-01.8	08 12	+11 25	1.055	0.138	62.5	KMTNet SAAO	<i>VR</i>
2021-04-03.1	08 11	+12 06	1.053	0.139	64.1	KMTNet CTIO	<i>VR</i>
2021-04-04.9	08 09	+13 00	1.049	0.142	66.2	CAHA 1.23 m	<i>R</i>
2021-04-05.4	08 08	+13 15	1.048	0.142	66.7	KMTNet SSO	<i>VR</i>
2021-04-05.9	08 08	+13 30	1.047	0.143	67.3	CAHA 1.23 m	<i>R</i>
2021-04-08.4	08 06	+14 39	1.042	0.146	70.1	KMTNet SSO	<i>VR</i>
2021-04-08.8	08 06	+14 50	1.041	0.147	70.6	KMTNet SAAO	<i>VR</i>
2021-04-14.8	08 02	+17 22	1.026	0.154	77.1	KMTNet SAAO	<i>VR</i>
2021-04-16.8	08 02	+18 09	1.021	0.156	79.2	KMTNet SAAO	<i>VR</i>
2021-04-18.4	08 01	+18 45	1.017	0.158	80.8	KMTNet SSO	<i>VR</i>
2021-04-18.8	08 01	+18 54	1.016	0.158	81.2	KMTNet SAAO	<i>VR</i>
2021-04-20.4	08 01	+19 29	1.012	0.160	82.9	KMTNet SSO	<i>VR</i>
-Sparse Photometry-							
2020-11-12	2021-04-09					ATLAS	<i>c</i>
2020-12-01	2021-04-03					ATLAS	<i>o</i>
-Space-based Photometry-							
2021-02-19	2021-03-07					TESS	wide <i>I</i>

Notes. R. A. : Right ascension, Dec. : Declination, Δ : geocentric distance, r_h : heliocentric distance, α : phase angle.

Table A.2. List of the historical light curves.

Date UT	R. A. (h m)	Dec. (° ')	r_h (AU)	Δ (AU)	α (°)	References
2012-12-23.3	10 42	-27 22	1.000	0.102	77.6	Pravec et al. (2014)
2012-12-25.3	10 33	-27 23	1.006	0.101	74.3	Pravec et al. (2014)
2012-12-26.3	10 28	-27 23	1.009	0.101	72.7	Pravec et al. (2014)
2012-12-27.2	10 23	-27 21	1.011	0.101	71.2	Pravec et al. (2014)
2012-12-28.2	10 18	-27 19	1.014	0.100	69.5	Pravec et al. (2014)
2012-12-29.2	10 13	-27 14	1.017	0.100	67.8	Pravec et al. (2014)
2012-12-30.2	10 08	-27 10	1.019	0.099	66.2	Pravec et al. (2014)
2012-12-31.2	10 03	-27 03	1.022	0.099	64.5	Pravec et al. (2014)
2013-01-03.2	09 47	-26 34	1.029	0.098	59.5	Pravec et al. (2014)
2013-01-04.2	09 41	-26 20	1.032	0.097	57.9	Pravec et al. (2014)
2013-01-05.2	09 36	-26 06	1.034	0.097	56.2	Pravec et al. (2014)
2013-01-06.1	09 30	-25 51	1.036	0.097	54.7	Pravec et al. (2014)
2013-01-06.2	09 30	-25 49	1.036	0.097	54.6	Pravec et al. (2014)
2013-01-07.2	09 24	-25 30	1.039	0.097	52.9	Pravec et al. (2014)
2013-01-07.6	09 22	-25 22	1.040	0.097	52.3	Pravec et al. (2014)
2013-01-08.1	09 19	-25 11	1.041	0.097	51.5	Pravec et al. (2014)
2013-01-08.1	09 19	-25 11	1.041	0.097	51.5	Pravec et al. (2014)
2013-01-08.2	09 18	-25 10	1.041	0.097	51.3	Pravec et al. (2014)
2013-01-09.1	09 13	-24 49	1.043	0.097	49.9	Pravec et al. (2014)
2013-01-09.1	09 13	-24 49	1.043	0.097	49.9	Pravec et al. (2014)
2013-01-09.2	09 12	-24 46	1.043	0.097	49.7	Pravec et al. (2014)
2013-01-09.3	09 12	-24 44	1.043	0.097	49.5	Pravec et al. (2014)
2013-01-10.1	09 07	-24 24	1.045	0.097	48.3	Pravec et al. (2014)
2013-01-10.2	09 06	-24 22	1.045	0.097	48.1	Pravec et al. (2014)
2013-01-10.3	09 06	-24 19	1.046	0.097	48.0	Pravec et al. (2014)
2013-01-11.1	09 01	-23 57	1.047	0.097	46.7	Pravec et al. (2014)
2013-01-11.3	09 00	-23 52	1.048	0.097	46.4	Pravec et al. (2014)
2013-01-11.5	08 59	-23 46	1.048	0.097	46.1	Pravec et al. (2014)
2013-01-12.1	08 55	-23 28	1.049	0.097	45.2	Pravec et al. (2014)
2013-01-12.2	08 55	-23 25	1.050	0.097	45.1	Pravec et al. (2014)
2013-01-12.2	08 55	-23 25	1.050	0.097	45.1	Pravec et al. (2014)
2013-01-13.1	08 49	-22 57	1.051	0.097	43.7	Pravec et al. (2014)
2013-01-13.2	08 49	-22 54	1.052	0.097	43.6	Pravec et al. (2014)
2013-01-14.1	08 44	-22 24	1.053	0.097	42.3	Pravec et al. (2014)
2013-01-14.1	08 44	-22 24	1.053	0.097	42.3	Pravec et al. (2014)
2013-01-14.2	08 43	-22 20	1.054	0.097	42.2	Pravec et al. (2014)
2013-01-15.1	08 38	-21 49	1.055	0.098	40.9	Pravec et al. (2014)
2013-01-15.2	08 37	-21 45	1.056	0.098	40.8	Pravec et al. (2014)
2013-01-15.5	08 35	-21 34	1.056	0.098	40.4	Pravec et al. (2014)
2013-01-16.1	08 32	-21 12	1.057	0.098	39.6	Pravec et al. (2014)
2013-01-16.1	08 32	-21 12	1.057	0.098	39.6	Pravec et al. (2014)
2013-01-16.3	08 31	-21 04	1.058	0.098	39.4	Pravec et al. (2014)
2013-01-16.3	08 31	-21 04	1.058	0.098	39.4	Pravec et al. (2014)
2013-01-19.1	08 15	-19 11	1.063	0.100	36.2	Pravec et al. (2014)
2013-01-19.2	08 15	-19 07	1.063	0.100	36.1	Pravec et al. (2014)
2013-01-20.1	08 10	-18 28	1.065	0.101	35.2	Pravec et al. (2014)
2013-01-20.2	08 10	-18 24	1.065	0.101	35.1	Pravec et al. (2014)
2013-01-22.2	07 59	-16 54	1.068	0.103	33.5	Pravec et al. (2014)
2013-01-22.3	07 59	-16 50	1.068	0.103	33.5	Pravec et al. (2014)
2013-01-23.1	07 55	-16 13	1.070	0.104	33.0	Pravec et al. (2014)
2013-01-23.2	07 55	-16 08	1.070	0.104	32.9	Pravec et al. (2014)
2013-01-24.1	07 50	-15 26	1.071	0.105	32.4	Pravec et al. (2014)
2013-01-24.2	07 50	-15 22	1.071	0.105	32.4	Pravec et al. (2014)
2013-01-24.3	07 49	-15 17	1.072	0.105	32.4	Pravec et al. (2014)
2013-02-04.1	07 10	-06 46	1.086	0.123	33.8	Pravec et al. (2014)
2013-02-05.1	07 07	-06 01	1.087	0.125	34.4	Pravec et al. (2014)
2013-02-05.3	07 07	-05 53	1.087	0.126	34.5	Pravec et al. (2014)
2013-02-06.1	07 05	-05 17	1.088	0.128	35.0	Pravec et al. (2014)
2013-02-06.2	07 04	-05 13	1.088	0.128	35.1	Pravec et al. (2014)

Table A.2. continued.

Date UT	R. A. (h m)	Dec. (° ′)	r_h (AU)	Δ (AU)	α (°)	References
2013-02-06.9	07 03	-04 43	1.089	0.129	35.5	Pravec et al. (2014)
2013-02-07.1	07 02	-04 34	1.089	0.130	35.7	Pravec et al. (2014)
2013-02-07.2	07 02	-04 29	1.089	0.130	35.7	Pravec et al. (2014)
2013-02-08.1	07 00	-03 51	1.090	0.132	36.4	Pravec et al. (2014)
2013-02-08.2	07 00	-03 47	1.090	0.132	36.4	Pravec et al. (2014)
2013-02-12.1	06 53	-01 09	1.093	0.142	39.3	Pravec et al. (2014)
2013-02-13.1	06 52	-00 31	1.094	0.145	40.1	Pravec et al. (2014)
2013-02-13.2	06 52	-00 27	1.094	0.145	40.2	Pravec et al. (2014)
2013-02-14.2	06 50	+00 10	1.094	0.148	40.9	Pravec et al. (2014)
2013-02-14.2	06 50	+00 10	1.094	0.148	40.9	Pravec et al. (2014)
2013-02-15.1	06 49	+00 43	1.095	0.150	41.6	Pravec et al. (2014)
2013-02-15.1	06 49	+00 43	1.095	0.150	41.6	Pravec et al. (2014)
2013-02-16.0	06 48	+01 15	1.095	0.152	42.3	Pravec et al. (2014)
2013-02-16.2	06 48	+01 22	1.096	0.153	42.5	Pravec et al. (2014)
2013-02-16.2	06 48	+01 22	1.096	0.153	42.5	Pravec et al. (2014)
2013-02-17.0	06 48	+01 49	1.096	0.155	43.0	Pravec et al. (2014)
2013-02-17.2	06 47	+01 56	1.096	0.156	43.2	Pravec et al. (2014)
2013-02-17.2	06 47	+01 56	1.096	0.156	43.2	Pravec et al. (2014)
2013-02-18.0	06 47	+02 23	1.096	0.158	43.8	Pravec et al. (2014)
2013-02-18.0	06 47	+02 23	1.096	0.158	43.8	Pravec et al. (2014)
2013-02-18.2	06 47	+02 30	1.096	0.159	44.0	Pravec et al. (2014)
2013-02-19.9	06 46	+03 25	1.097	0.163	45.2	Pravec et al. (2014)
2013-03-09.1	06 49	+10 38	1.096	0.215	56.3	Pravec et al. (2014)
2013-03-10.2	06 50	+11 00	1.095	0.218	56.9	Pravec et al. (2014)
2013-03-11.0	06 51	+11 15	1.095	0.221	57.3	Pravec et al. (2014)
2013-03-12.0	06 52	+11 33	1.094	0.224	57.9	Pravec et al. (2014)
2013-03-13.0	06 53	+11 51	1.094	0.227	58.4	Pravec et al. (2014)
2013-04-09.0	07 33	+17 20	1.060	0.297	70.7	Pravec et al. (2014)
2013-04-12.0	07 38	+17 43	1.054	0.303	71.9	Pravec et al. (2014)
2013-04-14.1	07 42	+17 57	1.050	0.307	72.8	Pravec et al. (2014)
2013-04-15.0	07 44	+18 03	1.048	0.308	73.2	Pravec et al. (2014)
2021-03-18.3	08 41	+02 08	1.080	0.120	42.9	Warner & Stephens (2021)
2021-03-19.2	08 38	+02 48	1.078	0.120	44.2	Warner & Stephens (2021)
2021-03-20.3	08 35	+03 37	1.077	0.122	45.8	Warner & Stephens (2021)
2021-03-21.2	08 33	+04 15	1.076	0.123	47.1	Warner & Stephens (2021)
2021-03-22.3	08 30	+05 01	1.074	0.124	48.7	Warner & Stephens (2021)
2021-03-23.3	08 28	+05 42	1.072	0.125	50.1	Warner & Stephens (2021)
2021-03-24.2	08 26	+06 19	1.071	0.126	51.4	Warner & Stephens (2021)
2021-03-27.2	08 20	+08 13	1.066	0.130	55.4	Warner & Stephens (2021)
2021-03-28.2	08 19	+08 50	1.064	0.131	56.7	Warner & Stephens (2021)
2021-03-29.2	08 17	+09 25	1.062	0.133	58.0	Warner & Stephens (2021)
2021-03-30.2	08 16	+09 59	1.060	0.134	59.3	Warner & Stephens (2021)
2021-03-31.2	08 14	+10 33	1.059	0.135	60.5	Warner & Stephens (2021)

Notes. R. A. : Right ascension, Dec. : Declination, Δ : geocentric distance, r_h : heliocentric distance, α : phase angle.

Appendix B: Light curves

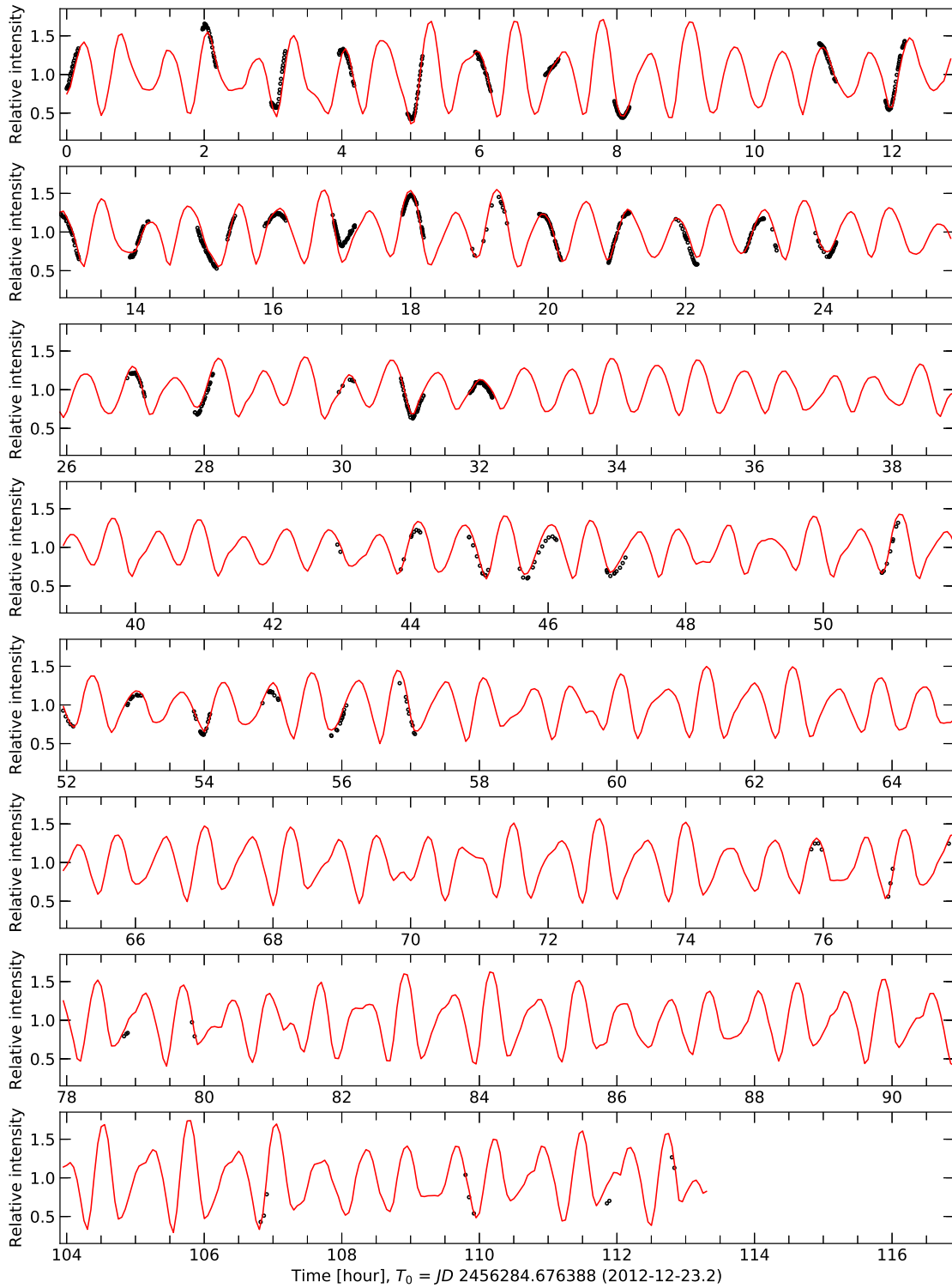


Fig. B.1. The photometric data in 2012-2013 (black open circle) with the synthetic light curve from best-fit model (red line).

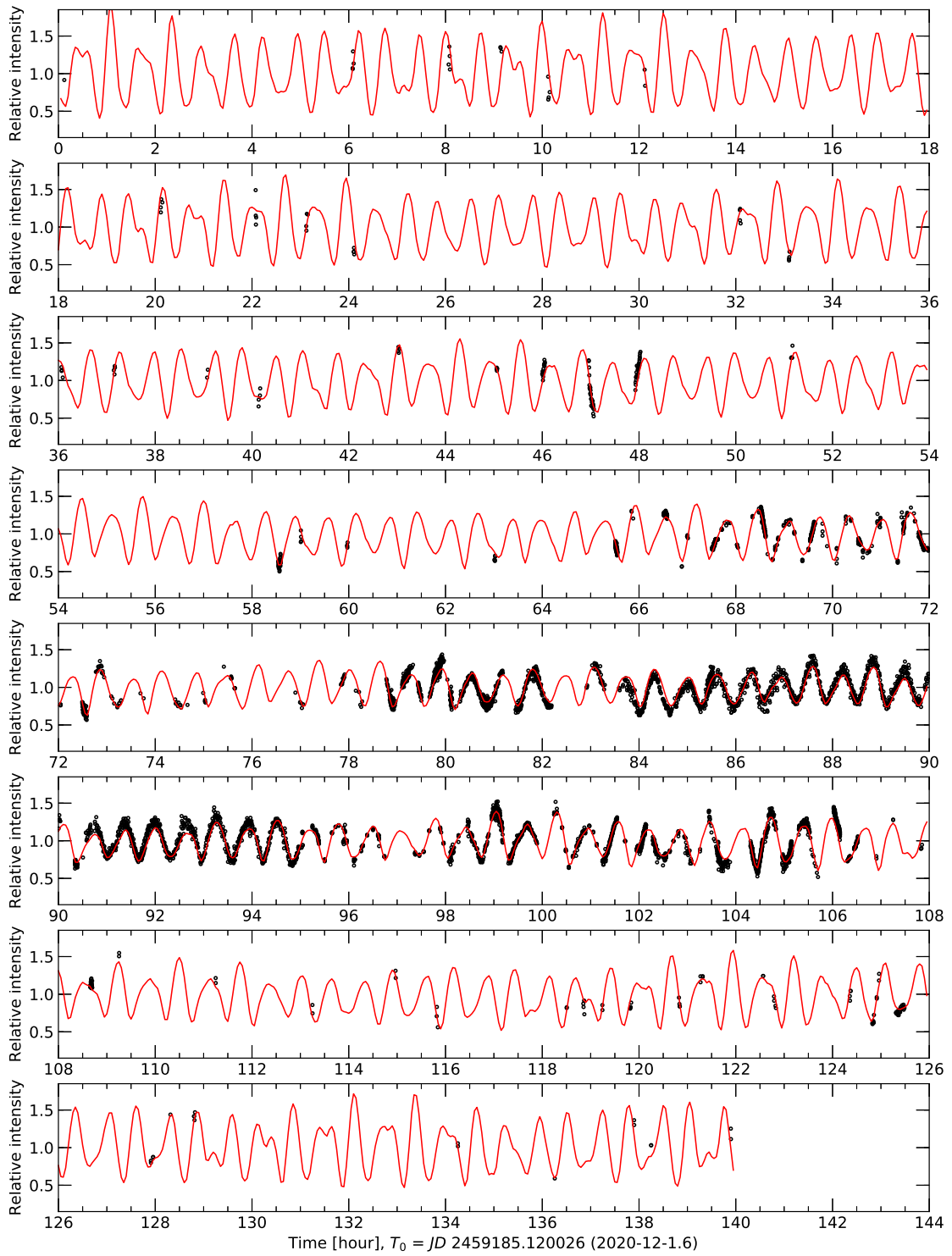


Fig. B.2. The photometric data in 2020-2021 (black open circle) with the synthetic light curve from best-fit model (red line).